Comput Mech (2016) 57:359–370
DOI 10.1007/s00466-015-1243-1

ORIGINAL PAPER

Thermodynamically consistent microstructure prediction of additively manufactured materials

Jacob Smith[1] · **Wei Xiong**[2] · **Jian Cao**[1] · **Wing Kam Liu**[1]

Received: 12 November 2015 / Accepted: 17 December 2015 / Published online: 5 January 2016

Abstract Additive manufacturing has risen to the top of research interest in advanced manufacturing in recent years due to process flexibility, achievability of geometric complexity, and the ability to locally modify and optimize materials. The present work is focused on providing an approach for incorporating thermodynamically consistent properties and microstructure evolution for non-equilibrium supercooling, as observed in additive manufacturing processes, into finite element analysis. There are two primary benefits of this work: (1) the resulting prediction is based on the material composition and (2) the nonlinear behavior caused by the thermodynamic properties of the material during the non-equilibrium solution is accounted for with extremely high resolution. The predicted temperature response and microstructure evolution for additively manufactured stainless steel 316L using standard handbook-obtained thermodynamic properties are compared with the thermodynamic properties calculated using the CALculation of PHAse Diagrams (CALPHAD) approach. Data transfer from the CALPHAD approach to finite element analysis is discussed.

✉ Wing Kam Liu
w-liu@northwestern.edu

Jacob Smith
jacobsmith2011@u.northwestern.edu

Wei Xiong
wxiong@yahoo.com

Jian Cao
jcao@northwestern.edu

[1] Department of Mechanical Engineering, Northwestern University, 2145 Sheridan Road, Evanston, IL 60208, USA

[2] Department of Material Science and Engineering, Northwestern University, 2220 Campus Drive, Evanston, IL 60208, USA

Keywords Additive manufacturing · Non-equilibrium solution · Finite element analysis · CALPHAD · Alloys

1 Introduction

Additive manufacturing (AM) is a materials processing method that dramatically improves the ability to design and create complex geometries in a layer-by-layer fashion. These methods are not limited to any particular material class, often incorporating polymeric, metallic, and biological materials. The scientific research community, especially in mechanical engineering and materials science, has begun to heavily focus efforts on advancing the state of metal-based AM methods. The reason for the recent peak in metal-based AM interest is because of the potential applications in development of low-volume application-specific structural components with optimized local and global thermodynamic and mechanical properties. The unique ability to alter local process parameters in order to obtain a desired microstructure conformation or local thermodynamic properties through establishment of process-structure-property relations is of particular interest.

AM processes have the potential to accelerate materials prototype design through fundamental metallurgical science (physical metallurgy, mechanical metallurgy and powder metallurgy), removal of design constraints on novel meta-materials, and simplification of developing functionally graded materials. However, the realization of novel AM processed materials and meta-materials in real-world applications has yet to come to fruition due to a lack of fundamental understanding of process-structure-property relations for AM processes. This lack of understanding is exaggerated compared to conventional subtractive processing techniques due to the inability to experimentally characterize important aspects of the process, such as the temperature

within the meltpool. To this end, utilization of computational frameworks that can inform the research community about complex phenomena in AM is a promising endeavor.

Previous work has been presented that takes advantage of finite element (FE) based heat transfer analysis to model AM processes [7,9,11,12,20,27,32,33,35]. Additional mathematical models [34] and finite element analysis (FEA) procedures [16,19] have been utilized to determine microstructure characteristics during AM process modeling. Additional references for mathematical and numerical modeling can be found in [16] and [26]. Li et al. [18] was able to experimentally connect thermodynamic properties to dendrite arm spacing (DAS) for Al-Cu-Mm alloys in the casting process. Subsequently, the DAS was linked to both experimental porosity and ultimate tensile strength, which shows a direct correlation between process, structure, and property. The most recent work of relevance to the present research was that by Amine et al. [1], which attempted to link direct laser deposition (DMD) process parameters to microstructure and material properties. This work was targeted primarily at determining a qualitative understanding of the microhardness and secondary dendrite arm spacing (SDAS) of stainless steel 316L (SS316L) resulting from variations in the process parameters. While this work is promising for understanding the effects of process parameters on microstructure and material properties, the modeling procedure used does not account for the composition of the material and quantitative predictions of microstructure and properties were not discussed; this is the research subject of the present work. By employing the CALPHAD method for fundamental alloy thermodynamics calculations in combination with FEA, the present first attempt interdisciplinary collaboration between mechanical engineering and materials engineering can provide composition-based process modeling as well as microstructure prediction.

The CALPHAD method has been established as a fundamental computational tool in investigation and design of multicomponent alloy materials [21,22,28]. The reason for this is because of the strong basis in thermodynamics and material kinetics of the CALPHAD method. Although it was originally developed for computational modeling of alloy thermodynamics based on the experimental phase equilibria and thermodynamic properties, it has since been extended to include the capability of modeling diffusion kinetics in inorganic materials [4]. The CALPHAD method is capable of predicting thermodynamically consistent properties for materials that have not yet been synthesized, making the method an excellent option for materials design [31]. Moreover, it can be used to quantitatively predict microstructural evolution through comprehensive physical models of materials processing. In order to perform spatially varying microstructure evolution simulations of materials, CALPHAD has recently been integrated with other modeling frameworks, e.g., phase field, to study process-structure relationships in three dimensions (3D) [17,30]. The CALPHAD method is particularly important for the present work due to the non-equilibrium supercooling behavior seen in AM processes.

The purpose of the present work is to provide a novel contribution to the AM research community that can be used to incorporate the impact of compositional alteration of powder used in AM process modeling. The resulting framework uses both thermodynamically consistent properties and quantitative microstructure predictions within a FE process modeling setting. Additionally, the proposed method offers a higher level of accuracy in predictions based on existing compositions, i.e., SS316L. The present work is organized as follows: Sect. 2 provides background information related to the CALPHAD method, Sect. 3 discusses the transfer of data obtained from the CALPHAD method into a format that is suitable for FEA, Sect. 4 describes the model setup used to predict the thermal response of the Electron Beam Melting (EBM) process, Sect. 5 showcases the results of an EBM example for SS316L, and Sect. 6 contains the concluding remarks of the manuscript.

2 The CALPHAD method

The CALPHAD approach is widely accepted in the materials research community as a powerful engineering method in materials thermodynamics and diffusion kinetics [5,15,22]. It was originally developed for computational modeling of alloy thermodynamics based on experimental phase equilibria and thermodynamic properties. A further development made in the CALPHAD research community enabled this approach to be applicable for diffusion kinetic modeling of inorganic systems [4]. The state-of-the-art CALPHAD method is one of the most significant methodologies in Materials Genome research, supporting both phase transformation modeling and materials property databases. The most significant advantage of the CALPHAD approach is the fidelity of model prediction for multicomponent alloys. For example, the CALPHAD thermodynamic calculations performed by Saunders [23] showed striking success in predicting phase transition temperatures, phase fractions, and many other thermodynamic properties of steel alloy systems.

Fundamentally, the CALPHAD model is based on the thermodynamic description of the pure elements, which is expressed as heat capacity starting from room temperature to temperatures much higher than the melting point for the material of interest. The standard CALPHAD database of the pure elements made by SGTE (Scientific Group Thermodata Europe) in 1991 [8] allows the CALPHAD community to perform CALPHAD-type thermodynamic modeling for binary, ternary and multicomponent alloy systems. The Gibbs free

energy of phase ϕ in a multicomponent alloy system G_m^ϕ can be defined using the CALPHAD model as:

$$G_m^\phi = \sum_i x_i^0 G_i^\phi + R\theta \left[\sum_i x_i \ln (x_i) \right] + {}^{Ex}G_m^\phi + {}^{Magn}G_m^\phi \quad (1)$$

in which R is the gas constant, θ is temperature, and x_i is the composition of element i in the multicomponent system. The third term on the right hand side (RHS) stands for excess energy in the system, which is a function of the interaction energy among atoms in different lattices. Thermodynamic models of solution phases, intermetallic compounds and oxides are developed based on the compound energy formalism [14], which serves as the fundamental theory of the CALPHAD approach. During the CALPHAD assessment, these interaction energies are defined as thermodynamic parameters, and are optimized according to phase diagrams and/or thermodynamic property data, which can be evaluated based on the reported measurements and atomistic modeling [29], e.g., density functional theory calculations. The last term on the RHS is an evaluation of the magnetic contribution to the total Gibbs energy [28], for which the magnetic transition temperature and local magnetic moments are considered as the input to evaluate magnetic entropy, and thus can be used to estimate spin magnetic energy. In order to apply the CALPHAD approach to materials design, (in addition to the database development) several comprehensive software have been developed, e.g., the Thermo-Calc software [2], which is generally considered as the pioneering software package in computational thermodynamics and kinetics.

One of the advantages in the CALPHAD method is its predictability of thermodynamic and kinetic properties of the multicomponent systems, which spans wide ranges of compositions and temperatures. Such a capability serves as a basis of performing diffusion kinetic simulations and non-equilibrium studies during the solidification process. By assuming local equilibrium status at the phase interface (note that the global solution is still considered a non-equilibrium process), the Scheil–Gulliver model [10,25] has been implemented in the Thermo-Calc software package for solidification simulation, which allows one to predict related thermodynamic property values for the solidification process. This model enables a qualitative analysis of the solute redistribution during solidification processes. It assumes that no diffusion takes place in the solid phases and that solute redistribution in the liquid is infinitely fast. As introduced by Scheil [25] in 1942, the partition coefficient, k, during solidification can be defined as the ratio of the local composition of the solid phase C_S to that of the liquid phase C_L, C_S/C_L. If C_0 is defined as the starting composition and f_S is the solid phase fraction, C_S can be obtained based on the following equation:

$$(C_L - C_S)\,\delta f_S = (1 - f_S)\,\delta C_L \quad (2)$$

Therefore, $C_S = kC_0\,(1 - f_S)^{k-1}$, which can be easily solved analytically in the case where the material evolves from liquid to a single solid phase. The CALPHAD approach further enables the solution when the complex phase transformations occur in multiphase and multicomponent systems. In modeling of solidification in steels, the back diffusion effect caused by fast diffusion species, such as carbon, has been further taken into account by Chen and Sundman [6] based on the CALPHAD approach. The Scheil–Gulliver simulation generates thermodynamic properties including latent heat and phase fraction during rapid cooling under the Scheil–Gulliver condition [6,24]. Therefore, the Scheil–Gulliver model available in the Thermo-Calc software is directly applied to obtain thermodynamic properties for the thermal modeling in the present work.

3 CALPHAD-based FEA for heat transfer

Based on the discussion in Sect. 2, it is clear that the CALPHAD method can provide a number of advantageous contributions to modeling of AM processes. However, the information provided by the CALPHAD method is based only on material composition and temperature, and thus lacks information related to the spatial distribution of the predicted properties or microstructural evolution; the use of a thermal modeling method coupled with the outputs from the CALPHAD method can be used in order to obtain the desired spatial distribution of the properties and microstructure. The goal of the present work is to develop a framework that will allow the thermodynamically consistent properties and microstructure afforded by the CALPHAD method to be used in analysis of an AM processed 3D domain. To this end, FEA is an obvious choice of modeling methodologies that can be implemented for multidimensional analysis. However, the data that is provided by the CALPHAD method in terms of the specific heat, the enthalpy change due to phase change, and the microstructure evolution must be transferred to a format that is suitable for FEA. In order to develop an appropriate approach for transferring this data, the governing equations that are solved in the FEA should be considered. The thermal equation that is to be solved in the present work can be written as follows,

$$\rho C_p^e\,(\theta)\,\frac{\partial \theta}{\partial t} = k\,(\theta)\,\nabla^2\theta + q_{app}\,(\mathbf{x}, t) + q_{rad}\,(\theta) \quad (3)$$

where θ is the temperature, ρ is the material density, C_p^e is the effective specific heat, which is a function of temperature, k is

the material conductivity, which is a function of temperature, q_{app} is the externally applied flux, which is a function of the spatial coordinates $\mathbf{x}$ and time t, and q_{rad} is the loss of heat due to radiation, which is a function of temperature. As the present work focuses on AM applications, the externally applied flux is assumed to be governed by a selected heat source model developed for either laser or electron beams. The heat source model used for the present work is a Gaussian surface flux model that can be written as,

$$q_{app} = \frac{-2\eta P}{\pi R_{beam}^2} \exp\left(-2\frac{R^2}{R_{beam}^2}\right) \tag{4}$$

where η is the absorption coefficient of the material, P is the laser/electron beam power, R_{beam} is the beam radius, and R is the radial distance from the heat source to the location of the material point of interest. A review of popular heat source models used for AM and welding applications can be found in [32]. The heat loss due to radiation is governed by the following equation,

$$q_{rad} = \sigma\varepsilon\left[(\theta - \theta_0)^4 - (\theta_\infty - \theta_0)^4\right] \tag{5}$$

where σ is the Stefan-Boltzmann constant, ε is the emissivity of the material, θ_0 is absolute zero temperature for the given thermal units, and θ_∞ is the ambient temperature.

Up to this point, the thermal model has been described but no consideration has been given to the integration of the CALPHAD-derived data and the governing equations. The thermodynamic information, e.g., enthalpy change and phase fraction, will be generated from the CALPHAD models as a function of temperature and material composition. The local thermodynamic information at a location in a 3D domain can be obtained so long as the temperature at that location is provided by the thermal model. It is assumed for the present study that the microstructure evolution equations obtained from the CALPHAD method will not directly affect the temperature or other state variables, i.e., the microstructure evolution equations will be directly calculated through a one-way coupling with the temperature. The microstructure evolution output from the CALPHAD method can therefore be fit by a polynomial function of the necessary order to replicate the behavior,

$$\phi_{phase}^{CALPHAD} = \sum_{n=1}^{p+1} a_n \theta^{p-n+1} \tag{6}$$

On the other hand, the specific heat and change in enthalpy due to phase change will be inherently integrated into the governing thermal equation through the effective specific heat described in Eq. 3. In particular, the effective specific heat is related to the enthalpy of the system through the following relationship,

$$C_p^e(\theta) = \frac{d(H + \Delta H)}{d\theta} = C_p(\theta) + \frac{d\Delta H}{d\theta} \tag{7}$$

where H represents the enthalpy of the system related to the specific heat with a constant phase and ΔH represents the additional energy of the system attributed to phase change. The traditional method of accounting for the phase change of the material is to obtain the specific heat and enthalpy change from an engineering handbook and simply apply them as follows,

$$C_p^e(\theta) = \begin{cases} C_p & \theta < \theta_S \\ C_p + \dfrac{\Delta H_L}{\theta_L - \theta_S} & \theta_S < \theta < \theta_L \\ C_p & \theta_L < \theta \end{cases} \tag{8}$$

where C_p is the handbook-obtained specific heat of the material (typically this value is constant or only valid to temperatures much lower than the solidus temperature), $\Delta H_L = \Delta H(\theta_L) - \Delta H(\theta_S)$ is the change in enthalpy of the system during the entire phase change using standard handbook properties (another name for this value is "latent heat" and it is typically treated as a constant, i.e., Eq. 8 implies that the contribution of phase change to Eq. 7 is constant), θ_S is the solidus temperature of the material, and θ_L is the liquidus temperature of the material. The additive form of the energy allows a fairly simple connection between the CALPHAD-based specific heat and enthalpy change due to phase evolution with that of the governing equations solved using FEA. For numerical efficiency, the authors have chosen to utilize a simple piece-wise constant relationship for the dependence of both the specific heat and the enthalpy change on temperature. The resulting equation, which is based on Eq. 8, can be written as follows,

$$C_p^e(\theta) = \begin{cases} C_p(\theta) & \theta < \theta_S \\ C_p(\theta) + \dfrac{d\Delta H}{d\theta} & \theta_S < \theta < \theta_L \\ C_p(\theta) & \theta_L < \theta \end{cases} \tag{9}$$

It should be noted that while the specific heat and change in enthalpy due to phase evolution are assumed constant for the handbook-based properties (Eq. 8), no such assumptions have been made in Eq. 9 (it is implied that ΔH is a function θ). As will be seen in later sections, the CALPHAD-based specific heat and change in enthalpy due to phase change can be quite nonlinear in temperature dependence. The temperature dependent nature of $C_p(\theta)$ and $dH/d\theta$ can be determined directly from the CALPHAD method outputs for a given material composition. In the ideal case, the specific heat outputs and the change in enthalpy due to phase transformation,

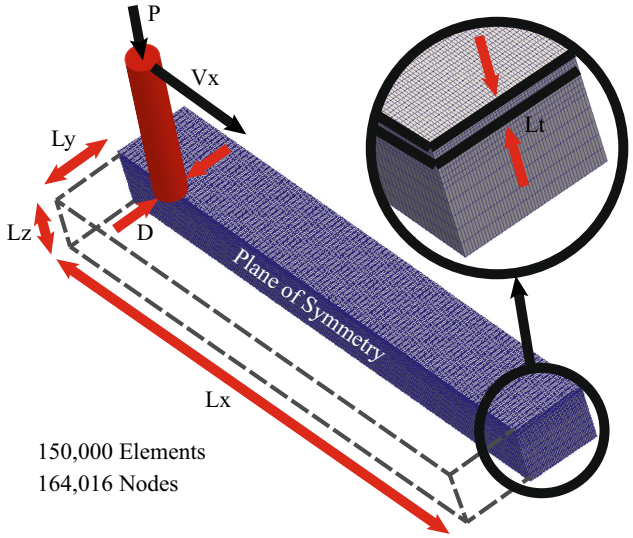

Fig. 1 Model setup for the powder bed FEA study

as obtained from CALPHAD, would be fitted to smooth functions and could be directly implemented in Eq. 9. The strong nonlinearity in the outputs is prohibitive for curve fitting the data, which is the reason for use of the much simpler piecewise constant model for the thermodynamic properties.

4 FEA model setup and assumptions

To compare the CALPHAD-derived properties with standard handbook properties the authors have developed a FE model of the EBM process. The model used for the present work is shown in Fig. 1. As can be seen in the figure, the model consists of 150,000 linear heat transfer hexahedral elements with 164,016 nodes. The plane of symmetry shown in the figure is located at the midpoint of the axis of the beam, which scans the domain parallel to the plane of symmetry. This model is indicative of a single track AM process for simplicity but there is no limitation of the proposed methodologies to such simplifications. The dimension Lx, Ly, and Lz are the length, width, and height of the domain, respectively, while the dimension Lt represents the thickness of the current layer in the EBM process. The parameters P and Vx are the beam power and velocity, respectively. The dimensions and process parameters used for the present work are shown in Table 1. All simulations were conducted using an in-house FE software that was developed by the first author. The average simulation time for the model shown in Fig. 1 for the CALPHAD-based solution was around 25 minutes using a single processor. The handbook-based solution was completed in around 7 minutes using a single processor.

Table 1 Dimensions and process parameters for the powder bed FEA study

Lx (mm)	Ly (mm)	Lz (mm)	Lt (mm)	Vx (mm/s)
4.0	0.5	0.4	0.05	100

It should be noted that powder bed based AM processes have an added complexity over the direct deposition processes in that the powder bed itself has dynamic thermal properties. In particular, the powder bed initially has a low conductivity compared with that of the bulk material or substrate. The powder bed properties must be accounted for in analysis because the thermal history in the heat affected zone is strongly dependent on the surrounding thermal influences, e.g., the surrounding powder bed. The methodology employed in the current work to obtain an accurate depiction of the impact of the powder bed on the single track is to simply switch the thermodynamic properties from that of the discrete powder to that of a continuous material once the material has breached the liquidus temperature. The adjustment of the thermodynamic properties is governed by the following equation,

$$m = \begin{cases} 0 & t = t_0 \\ 0 & \theta(t_n) < \theta_S \text{ and } m(t_{n-1}) = 0 \\ 1 & \theta_S < \theta(t_n) \text{ or } m(t_{n-1}) = 1 \end{cases} \tag{10}$$

where t_0 represents the initial condition of the analysis, $\theta(t_n)$ represents the temperature at time t_n, and $m\ (t_{n-1})$ represents the value of m itself at the previous time step. The parameter m will be referred to in subsequent sections as the material state parameter. Inspection of Eq. 10 implies that m simply acts as an on-off switch for the thermodynamic properties. Moreover, m can only shift in one direction, i.e., m can only be adjusted from 0 to 1, never 1 to 0. With this in mind, the equation for the evolution of the powder bed properties can be written as,

$$k\,(\theta) = m\ k_{bulk}\,(\theta) + (1 - m)\ k_{powder}\,(\theta) \tag{11}$$

where k_{bulk} and k_{powder} are the thermal conductivities of the bulk material and powder material, respectively. Based on Eqs. 10 and 11, it should now be clear that the thermal conductivity can only evolve in one direction, which is powder to bulk.

5 Results for SS316L

In order to showcase the capabilities provided by the CALPHAD-based heat transfer analysis, a powder bed example for EBM has been conducted using SS316L. The developed methodology, as explained in Sect. 3, requires

Table 2 CALPHAD material composition inputs for SS316L (wt.%)

Fe	Cr	Ni	Mo	Mn
Balance	16.3	10.3	2.09	1.31
Si	C	P	S	
0.49	0.026	0.026	0.006	

calculation of the thermodynamic properties of the material based on composition and temperature using CALPHAD and then transfer to a suitable data format for FEA. The temperature history, heating/cooling rate, and material phases are analyzed for the case study. Additionally, the SDAS is predicted at a given location based on a previously developed phenomenological law [36]. The variation in the predicted temperature history and microstructure evolution between the handbook-obtained [3] and CALPHAD-derived thermodynamic properties is discussed.

5.1 CALPHAD predictions for SS316L with non-equilibrium supercooling

The solidification behavior observed in AM processes is characterized by supercooling and the non-equilibrium solution is required in order to obtain accurate thermodynamic property predictions, which can be obtained by using the CALPHAD method. The composition of the powder, which was used as inputs to the CALPHAD prediction, is shown in Table 2. It should be noted that the handbook values for commercial alloys are usually rough estimations obtained for limited (if not fixed) temperature ranges. However, the CALPHAD method often provides thermodynamic/kinetic properties corresponding to a specific alloy composition from room temperature to well-above the alloy melting temperature. The CALPHAD model predictions in the current work were obtained by using the TCFE version 8 thermodynamic database for steels released by the Thermo-Calc software company. This database is generally considered as a highly accurate thermodynamic database for steels research.

The primary CALPHAD outputs of interest for this study are the heat capacity as a function of temperature, the change in enthalpy due to phase change as a function of temperature, and the phase evolution as a function of temperature. Fig. 2 shows a comparison of the CALPHAD outputs for the thermodynamic properties with the properties determined from the engineering handbook. It is clear from the figure that both the specific heat (Fig. 2a) and the change in enthalpy (Fig. 2b) are highly nonlinear for the CALPHAD outputs, while the handbook-obtained properties are linear or constant in the temperature dependence. The solidus and liquidus temperature lines in Fig. 2 are predicted using the CALPHAD method

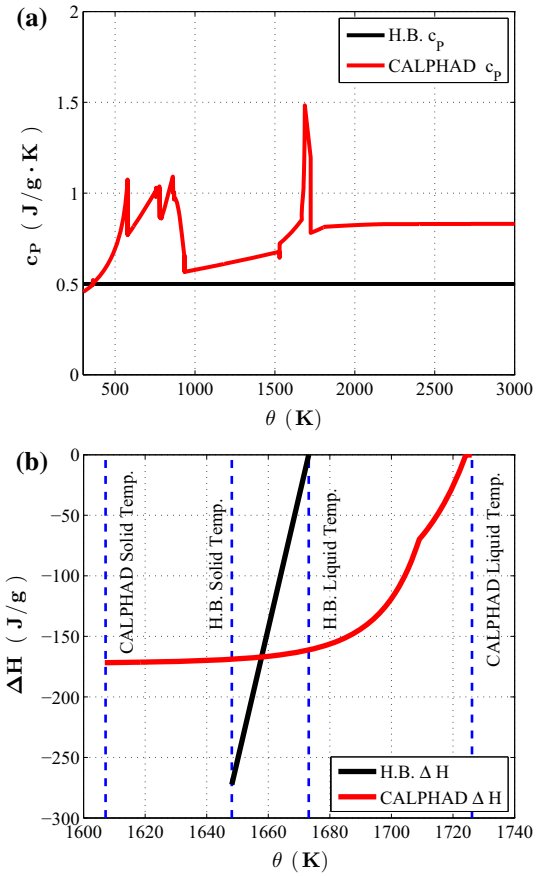

Fig. 2 Comparison of handbook-obtained and CALPHAD-derived temperature-dependent specific heat and change in enthalpy due to phase evolution for SS316L. **a** Specific heat as a function of temperature. **b** Change in enthalpy due to phase evolution as a function of temperature (solidus and liquidus temperatures derived from CALPHAD and the engineering handbook-based values are shown in Tables 3 and 8, respectively)

Table 3 Solidus and liquidus temperatures for SS316L based on CALPHAD output

θ_S (K)	θ_L (K)
1607.15	1726.15

based on the material composition (these values can be found in Table 2).

The reason for the simplified nature of the handbook-obtained properties is that there are difficulties in experimentally obtaining thermodynamic properties of multicomponent alloys over wide composition and temperature ranges. However, the nature of AM processes depends heavily on the accuracy of the thermodynamic properties because of the highly localized and complex phenomena involved in the solidification process, e.g., supercooling. The CALPHAD method offers a well-established alternative to experimental methods because the CALPHAD thermodynamic parameters are optimized based on evaluation of measured thermodynamic properties. Due to the fidelity of the CALPHAD

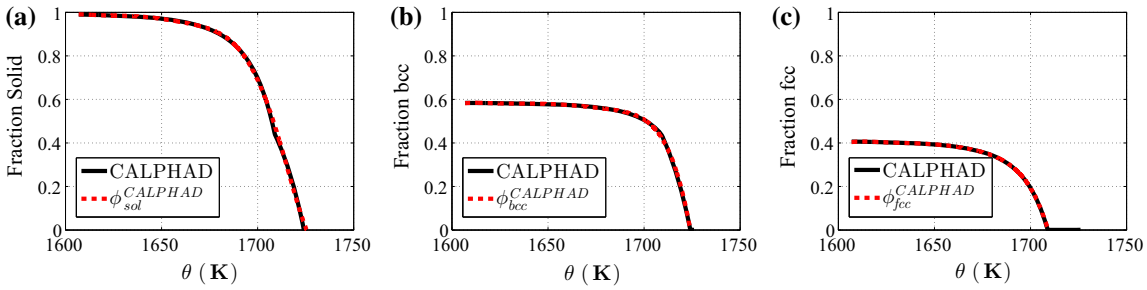

Fig. 3 The Scheil–Gulliver model prediction through the CALPHAD approach and polynomial fit as a function of temperature for SS316L. **a** Solid fraction as a function of temperature. **b** Fraction of bcc as a function of temperature. **c** Fraction of fcc as a function of temperature

model-prediction, it is well-respected as one of the most powerful techniques in developing new materials [21,22].

The solid (Fig. 3a), bcc (Fig. 3b), and fcc (Fig. 3c) phase evolution as a function of temperature predicted using the CALPHAD method is shown in Fig. 3. It should be noted that the solid fraction ranges from 0 to 1, 0 representing 100 % liquid phase and 1 representing 100 % solid phase. The sum of the bcc and fcc phase fractions is near unity when the solid fraction is 1, implying that the bcc and fcc phases represent almost 100 % of the solidified material. As expected, when the solid fraction is 0 the sum of the bcc and fcc phase fractions is also 0 - the material cannot have bcc and fcc phases in liquid form. Figure 3 also shows the polynomial functions that are used to fit data obtained using the CALPHAD method for the phases of the material during the solidification process. The polynomial equations used for replicating the solid fraction and bcc/fcc phase fractions (see Eq. 6) are shown in Eqs. 12 and 13, respectively.

$$\phi_{sol}^{CALPHAD} = b_1\theta^7 + b_2\theta^6 + b_3\theta^5 + b_4\theta^4 + b_5\theta^3 + b_6\theta^2 + b_7\theta + b_8 \quad (12)$$

$$\phi_{bcc/fcc}^{CALPHAD} = a_1\theta^6 + a_2\theta^5 + a_3\theta^4 + a_4\theta^3 + a_5\theta^2 + a_6\theta + a_7 \quad (13)$$

The selected polynomial coefficients for the solid fraction and bcc/fcc phase fractions are shown in Tables 4 and 5, respectively.

Table 4 Coefficients used for the fraction solid based on the CALPHAD output

b_1	1.28813813274e−13
b_2	−1.49189041117e−9
b_3	7.40432385162e−6
b_4	−2.04132708365e−2
b_5	33.7631277949
b_6	−33502.4090752
b_7	18466701.5972
b_8	−4361929680.48

Table 5 Coefficients used for the phase fraction of bcc and fcc based on the CALPHAD output

	bcc	*fcc*
a_1	−4.96066749054e−12	−5.27403300054e−12
a_2	4.91294422407e−8	5.21485553059e−8
a_3	−2.02723638189e−4	−2.14841171100e−4
a_4	4.46105544407e−1	4.72039262784e−1
a_5	−552.160313604	−583.374650716
a_6	364471.163322	384504.700626
a_7	−100235482.851	−105591780.663

Table 6 Heat source model parameters

P (W)	η	R_{beam} (mm)
60.0	0.6	0.175

Table 7 Radiation boundary condition parameters

σ (W/mm$^2K^4$)	ε	θ_0 (K)	θ_∞ (K)
5.6704e-14	0.2	0.0	300.0

5.2 Thermal history comparison between handbook properties and CALPHAD-derived properties

The thermal history and heating/cooling rates based on the thermodynamically consistent properties, which were derived using the CALPHAD method, are the primary quantities of interest; both the temperature and cooling rate govern the evolution of the microstructural phases of the material during solidification. Therefore, the present section provides a comparison between the handbook-obtained and the thermodynamically consistent properties for the temperature and the rate of change of temperature as a function of time. The FE model for the EBM process shown in Fig. 1 was used for the study. The heat source model parameters (see Eq. 4) are shown in Table 6, followed by the radiation boundary condition parameters (see Eq. 5) in Table 7.

Table 8 Model inputs for the powder bed FEA study based on handbook properties [3]

θ_S	θ_L	c_P	ΔH_L	ρ
1648.15	1673.15	0.5	272.5	0.008
(K)	(K)	$(J/g \cdot K)$	(J/g)	(g/mm^3)

Table 9 Thermal conductivity as a function of temperature and state for the CALPHAD informed solution

m	θ (K)	k (W/mm K)
0	0.0	0.0003
0	1607.15	0.0003
0	1726.15	0.0214
1	0.0	0.0214
1	1607.15	0.0214
1	1726.15	0.0214

Table 10 Thermal conductivity as a function of temperature and state for the handbook informed solution

m	θ (K)	k (W/mm K)
0	0.0	0.0003
0	1648.15	0.0003
0	1673.15	0.0214
1	0.0	0.0214
1	1648.15	0.0214
1	1673.15	0.0214

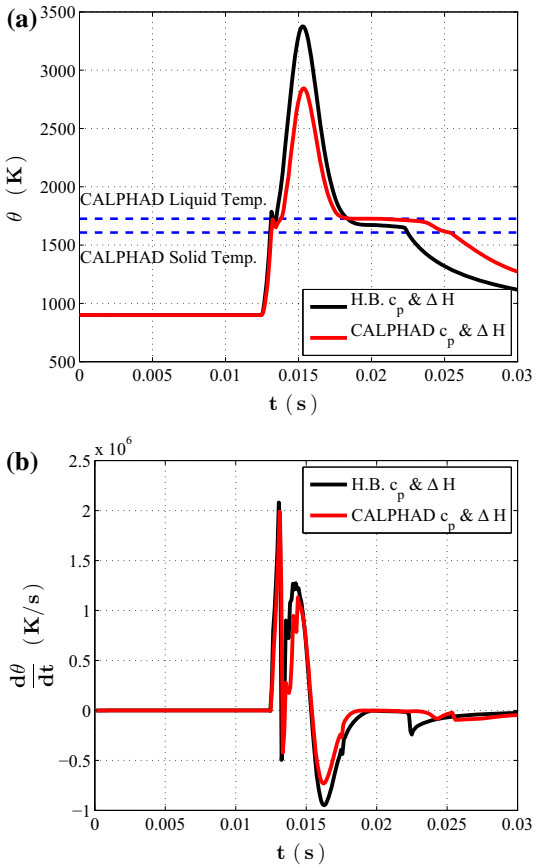

Fig. 4 Comparison of the response of a selected node predicted using the handbook-based property assumptions for specific heat and enthalpy change and those predicted by the CALPHAD method. **a** Thermal history for a selected node. **b** Temperature rate history for a selected node.

The thermodynamic properties obtained from the handbook are shown in Table 8. It should be noted that the material density (shown in Table 8) is assumed to be the same for both the handbook-based and CALPHAD-based solution. The density is further assumed to be constant in temperature dependence, despite the fact that the material switches from powder form, i.e., before melting, to a bulk material, i.e., after the material solidifies. Although this assumption is not ideal, it allows the methodology to be free of complications related to conservation of mass in the finite element solution.

The thermodynamic properties for the powder bed example evolve with both the temperature and the material state, which is either discrete powder or continuous; Eq. 10 is used to account for this via the state parameter, m, which has a one-way evolution. The thermal conductivity as a function of temperature and state for the CALPHAD informed solution and the handbook-based solution can be observed in Tables 9 and 10, respectively.

The temperature dependence of the thermal conductivity shown in Tables 9 and 10 could potentially have a higher resolution if it is provided; however, the resolution of the data is considered appropriate for the present study as it is primarily targeted at showcasing the potential impact of utilizing thermodynamically consistent properties predicted by the CALPHAD method - thermal conductivity is not one of these properties.

The temperature history (Fig. 4a) and heating/cooling (Fig. 4b) rate of a node that resides on the top surface of the powder bed and in the direct path of the electron beam are shown in Fig. 4. There is a noticeable difference in both the peak temperature and the heating/cooling rates predicted for the handbook-based and CALPHAD-based solutions. The CALPHAD-based properties yield a dramatic decrease in the peak temperature and reduce the peak rates of heating and cooling. The impact of the heating rate will be neglected from this point forward due to the fact that the cooling rate, i.e., $\mathrm{d}\theta/\mathrm{d}t < 0$ in Fig. 4b, is the primary output of interest for determining the evolution of the as-built microstructure.

5.3 Microstructure prediction comparison between handbook properties and CALPHAD-derived properties

The microstructure evolution of the AM processed SS316L material will be analyzed in this section. By combining the CALPHAD method with FEA, the evolution of the as-built

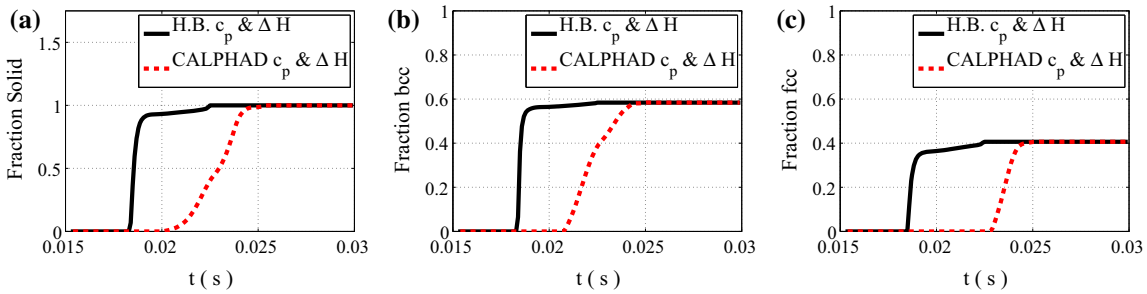

Fig. 5 Predicted phases at a selected node as a function of time based on the CALPHAD output. **a** Solid fraction as a function of time. **b** Fraction of bcc as a function of time. **c** Fraction of fcc as a function of time

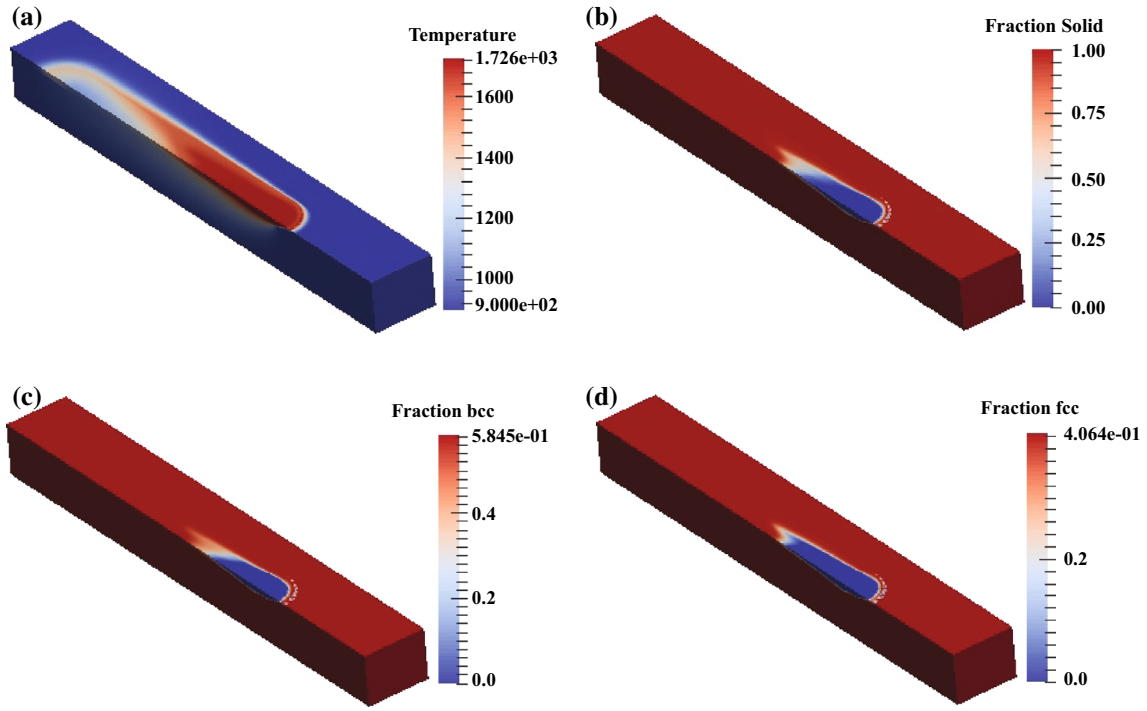

Fig. 6 Snapshots of the predicted temperature and phase distribution in the powder bed example using the CALPHAD informed properties. **a** Snapshot of the predicted temperature distribution. **b** Snapshot of the predicted solid fraction distribution. (c) Snapshot of the predicted bcc fraction distribution. **d** Snapshot of the predicted fcc fraction distribution

microstructure can be easily predicted locally at a node, or in a 3D distribution, based on the non-equilibrium solution and thermodynamically consistent properties (calculated considering supercooling behavior a priori). A comparison of the evolution of the phases in the material predicted using the handbook-based and CALPHAD-based properties at a specific node, which is the same node as that used to predict the thermal history in Fig. 4, is shown in Fig. 5. The predicted evolution of phases depicted in Fig. 5 are based on the polynomials shown in Eqs. 12 (fraction solid—Fig. 5a) and 13 (fraction bcc/fcc—Figs. 5b and 5c, respectively). The nodal output for the two cases of properties is extremely different in both the time at which the material breaches the liquidus temperature during the cooling cycle, i.e., solidification behavior is initiated, and in the evolution of the phases. Despite the fact that the same equations are used to predict the phases, the thermal history of the handbook-based and CALPHAD-based solutions drive the behavior of the phase evolution.

The temporal differences in phase evolution between the two cases has an impact on the phase gradient in the material at a given snapshot in time. The 3D distributions of the temperature field (Fig. 6a) and the solid (Fig. 6b), bcc (Fig. 6c), and fcc (Fig. 6d) phase fraction fields at a snapshot in time for the CALPHAD-based solution are shown in Fig. 6. It should be noted that a cap corresponding to the liquidus temperature shown in Table 3 was set for the temperature field; therefore, the dark red in the figure represents the material in a liquid state to improve the visibility of the molten pool. The effect of the material state parameter (Eq. 10), which allows the

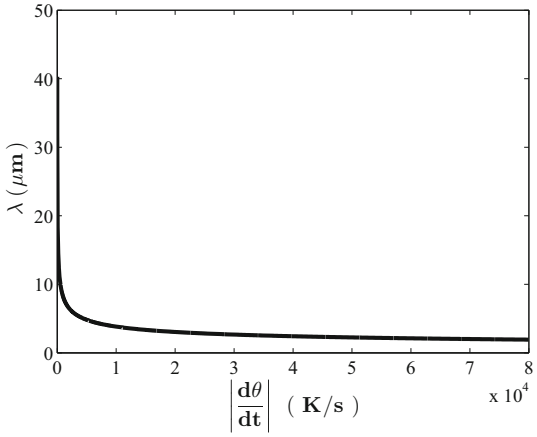

Fig. 7 SDAS as a function of temperature rate

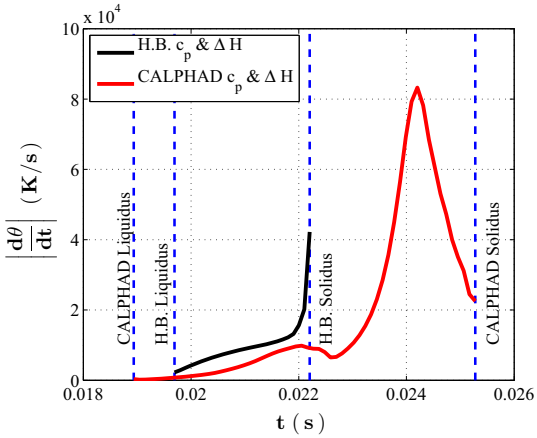

Fig. 8 Cooling rate history (magnitude) of a selected node during the solidification process

difference in the powder and continuum properties of SS316L to be accounted for in the powder bed process model, can be seen at the tail edge of the single track. The powder bed insulates the single track in such a way that heat cannot easily leave in the direction of the powder bed due to the low thermal conductivity.

Figures 6b through 6d show the distribution of the phases within the molten pool at a snapshot in time. By inspection of Fig. 6b, the dark red in the phase distribution figures represents the material in a completely solid form, while the dark blue represents the material in a completely liquid form. The sharp gradient in the predicted phase fraction distributions indicates the localized nature of the EBM heat source model. Using the 3D phase fraction prediction afforded by coupling CALPHAD-based thermodynamic properties with FEA, the heat source distribution and other process parameters, e.g., the scan speed of the beam, could easily be optimized to control the phase gradient in the single track for improved microstructural conformation and properties, which is a novel concept to the knowledge of the authors. For the first time, the effect of the evolution of solid, bcc, or

Table 11 SDAS predicted for the handbook-based and CALPHAD-based solution

	Handbook	CALPHAD
$\left\|\frac{d\theta}{dt}\right\|_e$ (K/s)	9.9529e+3	1.8719e+4
λ (μm)	3.8350	3.1108

fcc phase fraction on other microstructural state variables or mechanical properties can be accounted for in 3D within a product-scale process model.

As previously stated, another key microstructural parameter related to the mechanical properties of a material is SDAS. Zheng et al. [36] have previously developed a phenomenological relationship between the SDAS and the cooling rate (see Fig. 7) for SS316L,

$$\lambda = 80 \left|\frac{d\theta}{dt}\right|^{-0.33} \tag{14}$$

where λ is the SDAS. Using Eq. 14 and the results shown in Fig. 4b, the resulting SDAS can be predicted for a given set of process parameters. It should be noted that the equation shown for the SDAS is only relevant during the solidification phase. Moreover, the SDAS will require either an effective temperature rate through the solidification process (see Fig. 8) or an effective SDAS. The predicted SDAS for the handbook-based solution and the predicted SDAS for the CALPHAD-based solution are compared in Table 11. While it is unclear what the correct effective temperature rate or effective SDAS should be (due to a lack of sufficient experimental data), the authors have chosen to use an effective temperature rate approach for the current comparison study between the two solutions.

The predicted SDAS shown in Table 11 was calculated using the following effective cooling rate equation for the solidification process,

$$\left|\frac{d\theta}{dt}\right|_e = \left|\frac{\theta_S - \theta_L}{t_S - t_L}\right| \tag{15}$$

where t_S and t_L are the time at which the solidus and liquidus temperatures are reached during the solidification process, respectively. The discrepancy is substantial between the predicted SDAS for the handbook-based and CALPHAD-based solutions, having a percent difference of around 21%. Although a thorough quantitative comparison between the predicted SDAS values and experimental measurements will need to be conducted in the future, the difference in the values predicted using the handbook properties and the CALPHAD-derived thermodynamically consistent properties is sufficient to warrant further investigation in how material properties are derived for heat transfer analysis involving complex solidification behavior.

6 Conclusions

The localized nature of the energy input, cyclic phase changes, and rapid cooling rates establishes AM process modeling as a strongly materials science driven problem. Interdisciplinary research between mechanical engineers and metallurgists/materials engineers is vital to the success of AM processes. The current work presents a novel interdisciplinary CALPHAD-based heat transfer analysis by utilizing thermodynamically consistent properties in FEA. The transfer of data from the CALPHAD method to the FEA allows the 3D prediction of the phase evolution during complex solidification behavior. An additive manufacturing powder bed example, in which the standard handbook-based properties and the CALPHAD-derived properties have been compared, was used in order to showcase the potential advancement in the understanding of process-structure relationships for applications involving supercooling behavior. The distribution of the solid, bcc, and fcc phase fractions were elucidated based on the outputs from the CALPHAD method and a comparison of the predicted SDAS obtained from the handbook-based and CALPHAD-based property assumptions were discussed. The results conclusively show that there is a substantial difference between the predicted temperature response and microstructural evolution when using thermodynamically consistent properties and those obtained using handbook-based properties.

While the authors have shown a promising method for connecting CALPHAD-based thermodynamic property information to 3D FEA, further experimental calibration and validation is required. The primary difficulty is in model calibration and validation from the standpoint of the temperature near the melt pool. To the knowledge of the authors, there has yet to be a successful experimental method developed for accurately obtaining the temperature and thermal gradients near the melt pool (primarily due to the extremely high temperature ranges observed in AM processes and the localized nature of these processes). It should be noted that the current model could potentially be further improved if accurate measurements of the temperature profile were available for the extreme cooling/heating behavior in AM processes. For example, the solute trapping model [13] has a more accurate description of rapid solidification kinetics than that obtained from the Scheil–Gulliver model and could also be applied to FEA within the propsed framework. In addition, a more satisfactory model for superheating needs to be developed for AM processes, as compared with the local equilibria assumption currently used for the superheating behavior in AM.

Aside from the impact that the thermodynamically consistent properties can have on the microstructure prediction in AM processes, there could potentially be dramatic effects on the predicted thermal gradients and evaporation behavior. The thermal gradients in the material are important descriptors for determining the residual stresses in as-built AM materials. The prediction of evaporation behavior during the process can lead to the detection of both internal and surface porosity, which is detrimental to products with stringent demands on surface quality and fatigue life. An accurate prediction of the microstructure, the residual stresses, and the surface roughness could potentially lead to an enhanced understanding of the correlation between process parameters, microstructure, and final product properties and performance. The process-structure-property relationship is the key to process optimization and ubiquitous adoption of AM in industrial applications. Future work will be directed at prediction of residual stresses, porosity, and surface roughness using the presented thermodynamically consistent modeling method.

The connection between the CALPHAD method and the FE method has many applications. In particular, applications where a material is heated to temperatures above the solidus temperature and where non-equilibrium supercooling behavior is observed. Aside from the aforementioned further development of the CALPHAD-based thermodynamic property predictions, future work of the authors is to apply the methodology presented here to other material compositions and other processes. This method can have a tremendous impact in understanding the process-structure relationship for many processes involving multicomponent alloys, e.g., selective laser melting (SLM) and laser engineered net shaping (LENS).

Acknowledgments The authors would like to gratefully acknowledge the support for this work provided by National Institute of Standards and Technology (NIST) and Center for Hierarchical Materials Design (CHiMaD) under Grant No. 70NANB13Hl94 and 70NANB14H012. The first author would like to acknowledge the United States Department of Defense for their support through the National Defense Science and Engineering Graduate (NDSEG) fellowship award. Wei Xiong is grateful to the Thermo-Calc software company for providing the license to the software and databases used in this research.

References

1. Amine T, Newkirk JW, Liou F (2014) An investigation of the effect of direct metal deposition parameters on the characteristics of the deposited layers. Case Stud Therm Eng 3:21–34. doi:10.1016/j.csite.2014.02.002. http://www.sciencedirect.com/science/article/pii/S2214157X14000070
2. Andersson JO, Helander T, Höglund L, Shi P, Sundman B (2002) Thermo-Calc & DICTRA, computational tools for materials science. Calphad 26(2):273–312. doi:10.1016/S0364-5916(02)00037-8
3. AZoM.com: AZO Materials: Stainless Steel - Grade 316 (UNS S31600) (2015). http://www.azom.com/properties.aspx?ArticleID=863
4. Borgenstam A, Höglund L, Ågren J, Engström A (2000) Dictra, a tool for simulation of diffusional transformations in alloys. J Ph Equilib 21(3):269–280. doi:10.1361/105497100770340057

5. Chang Y, Chen S, Zhang F, Yan X, Xie F, Schmid-Fetzer R, Oates W (2004) Phase diagram calculation: past, present and future. Prog Mater Sci 49(34):313–345. doi:10.1016/S0079-6425(03)00025-2. http://www.sciencedirect.com/science/article/pii/S0079642503000252
6. Chen Q, Sundman B (2002) Computation of partial equilibrium solidification with complete interstitial and negligible substitutional solute back diffusion. Mater Trans 43(3):551–559. doi:10.2320/matertrans.43.551
7. Dai K, Shaw L (2004) Thermal and mechanical finite element modeling of laser forming from metal and ceramic powders. Acta Mater 52(1):69–80. doi:10.1016/j.actamat.2003.08.028. http://www.sciencedirect.com/science/article/pii/S1359645403005081
8. Dinsdale A (1991) SGTE data for pure elements. Calphad 15(4):317–425. doi:10.1016/0364-5916(91)90030-N. http://www.sciencedirect.com/science/article/pii/036459169190030N
9. Foroozmehr A, Badrossamay M, Foroozmehr E, Golabi S (2016) Finite element simulation of selective laser melting process considering optical penetration depth of laser in powder bed. Mater Des 89:255–263. doi:10.1016/j.matdes.2015.10.002. http://www.sciencedirect.com/science/article/pii/S0264127515305803
10. Gulliver G (1913) The quantitative effect of rapid cooling upon the constitution of binary alloys. J Inst Met 9:120–157
11. Gusarov A, Smurov I (2010) Modeling the interaction of laser radiation with powder bed at selective laser melting. Phys Proced, vol 5, part B. In: Laser sssisted net shape engineering 6, proceedings of the LANE 2010, part 2, pp 381–394. doi:10.1016/j.phpro.2010.08.065. http://www.sciencedirect.com/science/article/pii/S1875389210004918
12. Gusarov AV, Yadroitsev I, Bertrand P, Smurov I (2009) Model of radiation and heat transfer in laser-powder interaction zone at selective laser melting. J Heat Transf 131(7):072101. doi:10.1115/1.3109245
13. Hillert M (1999) Solute drag, solute trapping and diffusional dissipation of gibbs energy. Acta Mater 47(18):4481–4505. doi:10.1016/S1359-6454(99)00336-5. http://www.sciencedirect.com/science/article/pii/S1359645499003365
14. Hillert M (2001) The compound energy formalism. J Alloys Compd 320(2):161–176. doi:10.1016/S0925-8388(00)01481-X
15. Kaufman L, Ågren J (2014) Calphad, first and second generation birth of the materials genome. Scr Mater 70:3–6. doi:10.1016/j.scriptamat.2012.12.003. http://www.sciencedirect.com/science/article/pii/S1359646212007749
16. King W, Anderson A, Ferencz R, Hodge N, Kamath C, Khairallah S (2015) Overview of modelling and simulation of metal powder bed fusion process at lawrence livermore national laboratory. Mater Sci Technol 31(8):957–968
17. Kitashima T (2008) Coupling of the phase-field and CALPHAD methods for predicting multicomponent, solid-state phase transformations. Philos Mag 88(11):1615–1637. doi:10.1080/14786430802243857
18. Li Q, Chen Y, Jiang Z (1985) Relationship between solidification thermal parameters and dendrite arm spacing and ultimate tensile strength in Al-Cu-Mm alloys. J Less Common Met 110(1):171–174. doi:10.1016/0022-5088(85)90318-2. http://www.sciencedirect.com/science/article/pii/0022508885903182
19. Manvatkar V, De A, DebRoy T (2015) Spatial variation of melt pool geometry, peak temperature and solidification parameters during laser assisted additive manufacturing process. Mater Sci Technol 31(8):924–930. doi:10.1179/1743284714Y.0000000701
20. Matsumoto M, Shiomi M, Osakada K, Abe F (2002) Finite element analysis of single layer forming on metallic powder bed in rapid prototyping by selective laser processing. Int J Mach Tools Manuf 42(1):61–67. doi:10.1016/S0890-6955(01)00093-1. http://www.sciencedirect.com/science/article/pii/S0890695501000931
21. Olson GB (2013) Genomic materials design: the ferrous frontier. Acta Mater 61(3):771–781. doi:10.1016/j.actamat.2012.10.045. http://www.sciencedirect.com/science/article/pii/S1359645412007926
22. Olson GB, Kuehmann CJ (2014) Materials genomics: from calphad to flight. Scr Mater 70:25–30. doi:10.1016/j.scriptamat.2013.08.032. http://www.sciencedirect.com/science/article/pii/S1359646213004375
23. Saunders N (2009) The application of thermodynamic and material property modeling to process simulation of industrial alloys, metals process simulation. In: Furrer DU, Semiatin SL (eds) ASM Handbook, Vol 22B. ASM International, Materials Park, pp 132–153
24. Schaffnit P, Stallybrass C, Konrad J, Stein F, Weinberg M (2015) A scheilgulliver model dedicated to the solidification of steel. Calphad 48:184–188. doi:10.1016/j.calphad.2015.01.002. http://www.sciencedirect.com/science/article/pii/S0364591615000036
25. Scheil E (1942) Bemerkungen zur schichtkristallbildung. Zeitschrift fuer Metallkunde 34:70–72
26. Smith J, Xiong W, Yan W, Lin S, Cheng P, Kafka OL, Wagner GJ, Cao J, Liu WK (2015) Linking process, structure, property, and performance for metal based additive manufacturing: computational approaches with experimental support. Comput Mech. doi:10.1007/s00466-015-1240-4
27. Tolochko NK, Arshinov MK, Gusarov AV, Titov VI, Laoui T, Froyen L (2003) Mechanisms of selective laser sintering and heat transfer in ti powder. Rapid Prototyp J 9(5):314–326. doi:10.1108/13552540310502211
28. Xiong W, Chen Q, Korzhavyi PA, Selleby M (2012) An improved magnetic model for thermodynamic modeling. Calphad 39:11–20. doi:10.1016/j.calphad.2012.07.002. http://www.sciencedirect.com/science/article/pii/S0364591612000612
29. Xiong W, Du Y, Hu RX, Wang J, Zhang WW, Nash P, Lu XG (2008) Construction of the Al–Ni–Si phase diagram over the whole composition and temperature ranges: thermodynamic modeling supported by key experiments and first-principles calculations. Int J Mater Res 99:598–612. Kolbergerstrasse 22, Munchen, D-81679. doi:10.3139/146.101681
30. Xiong W, Grönhagen KA, Ågren J, Selleby M, Odqvist J, Chen Q (2011) Investigation of spinodal decomposition in Fe–Cr alloys: CALPHAD modeling and phase field simulation, pp 1060–1065. http://dx.doi.org/10.4028/www.scientific.net/SSP.172-174.1060
31. Xiong W, Olson GB (2015) Integrated computational materials design for high-performance alloys. MRS Bull 40(12):1035–1044. doi:10.1557/mrs.2015.273. http://www.journals.cambridge.org/abstract_S0883769415002730
32. Yan W, Smith J, Ge W, Lin F, Liu W (2015) Multiscale modeling of electron beam and substrate interaction: a new heat source model. Comput Mech 52:1–12. doi:10.1007/s00466-015-1170-1
33. Yin J, Zhu H, Ke L, Hu P, He C, Zhang H, Zeng X (2015) A finite element model of thermal evolution in laser micro sintering. Int J Adv Manuf Technol, pp 1–13. doi:10.1007/s00170-015-7609-x
34. Zaeh M, Ott M (2011) Investigations on heat regulation of additive manufacturing processes for metal structures. CIRP Ann Manuf Technol 60(1):259–262. doi:10.1016/j.cirp.2011.03.109. http://www.sciencedirect.com/science/article/pii/S0007850611001107
35. Zäh M, Lutzmann S (2010) Modelling and simulation of electron beam melting. Prod Eng 4(1):15–23. doi:10.1007/s11740-009-0197-6
36. Zheng B, Zhou Y, Smugeresky JE, Schoenung JM, Lavernia EJ (2008) Thermal behavior and microstructure evolution during laser deposition with laser-engineered net shaping: part II. Experimental investigation and discussion. Metall Mater Trans A 39(9):2237–2245. doi:10.1007/s11661-008-9566-6